Observation of hysteretic magnetic phase transitions coupled with orientation motion of ions and dielectric relaxation in a one-dimensional nickel-bis-dithiolene molecule solid

Xuan-Rong Chen,[a] Wei-Hua Ning,[a] Hao Yang,[a] Jian-Lan Liu,[a] Fang Xuan,[a] Xiao-Ming Ren*[abc]

[a] State Key Laboratory of Materials-Oriented Chemical Engineering and College of Science, Nanjing University of Technology, Nanjing 210009, P. R. China

[b] College of Materials Science and Engineering, Nanjing University of Technology, Nanjing 210009, P. R. China

[c] State Key Lab & Coordination Chemistry Institute, Nanjing University, Nanjing 210093, P. R. China

Tel.: +86 25 58139476

Fax: +86 25 58139481

Email: xmren@njut.edu.cn

Abstract

The second polymorph, β-crystal, of the nickel-bis-dithiolene compound [4'-CF_3bzPy][Ni(mnt)$_2$] where 4'-CF_3bzPy = 1-(4'-trifluoromethylbenzyl)pyridinium and mnt^{2-} = maleonitriledithiolate, was obtained. The variable-temperature single crystal structures, magnetic behavior in 1.8-300 K and dielectric nature in 123-373 K have been investigated for β-crystal. This polymorph experiences two hysteretic magnetic phase transitions in a narrow temperature region (190-217 K) with the thermal hysteresis loops ca. 7 K and ca. 11 K. Two hysteretic magnetic phase transitions are coupled with two isostructural phase transitions (IPTs), respectively, which are driven by the novel step-wise dynamic orientation motion of anion and cation in the β-crystal. There is absent dielectric anomaly in the structural transformation temperature interval. However, a dielectric relaxation, related to the dipole motion of polar CF_3 groups in the cations under an ac electrical field, emerges in the high-temperature phase.

Keywords: Nickel-bis-dithiolene; dynamic structural disorder; hysteretic magnetic transition; dielectric relaxation

Introduction

Polymorphism is one of the most fascinating phenomena of solid state chemistry and indeed is a “difficult” phenomenon. In spite of the huge efforts of many researchers our knowledge of this phenomenon is still embryonic, the relationship between growth of a crystalline phase and nucleation of the first crystallites is often mysterious,[1] and remains poorly understood, therefore, it is difficult to control and predict the emergence of different forms at present stage.[2] Polymorphs, usually, exhibit a range of different physico-chemical properties, which probably affect the application and utilization of the solid materials, owing to their distinct crystal arrangement.[3]

Ion-pair compounds comprised of the planar molecule architectures of metal-bis-1, 2-dithiolene as well as the oxidized derivatives of tetrathiafulvalene (TTF) have been widely studied for many years; this is due to their novel physical properties in the areas of magnetic[4, 5] and conducting[6, 7] materials. The planarity of these molecules promotes charge delocalization, thereby minimizing Coulombic repulsions; this allows π-π stacking of planar molecule architectures and the corresponding ion-pair compound tend to display rich structural polymorphism as well as related magnetic and electric properties.[8-11] From this view point, the isolation, identification and characterization of different polymorphs are very useful works for better understanding the factors that control the nucleation of polymorphic materials and the growth of the desired polymorph with fascinating magnetic or conducting property.

Recently, we reported the structural and magnetic properties of a magnetic bistable compound, [4’-CF_3bzPy][Ni(mnt)$_2$] (**1**) where mnt^{2-} = maleonitriledithiolate and 4’-CF_3bzPy$^+$ = 1-(4’-trifluoromethylbenzyl)pyridinium.[12] The ion-pair crystal of **1** was built up of the mixed stacks. The [Ni(mnt)$_2$]$^-$ dimers and 4’-CF_3bzPy$^+$ dimers form the alternating arrangement within a mixed stack and the fluorine atoms in CF_3 group of cation show structurally disordered at room temperature. It is surprising that the disorder-to-order transformation of CF_3 group together with the relative dislocation of the neighboring molecule layers undergo around 159 K in the cooling process and these structural transformations cooperate with a bistable magnetic phase transition with a surprising wide thermal hysteresis loop (~49 K).[12]

In this study, we report a new polymorph of **1**, and this new polymorph possesses three crystalline phases within a very narrow temperature interval and two structural phase transitions are associated with novel hysteretic magnetic transitions. For convenience, the previously reported and the new polymorphs of ion-pair compound **1** are sequentially labeled as **α**- and **β**-crystal, respectively. Herein, we present the investigations of crystal structural, magnetic and dielectric properties of **β**-crystal.

Experimental

Chemicals and Materials

The staring materials, Na_2mnt[13] and [4'-CF_3bzPy]Cl,[14] were synthesized following the reported method in the literatures. [4'-CF_3bzPy][Ni(mnt)$_2$] (**1**) was prepared using our previous reported procedure.[12]

β-crystals were grown from the slow evaporation of the saturated acetone solution of **1** with a little amount of isopropanol at ambient temperature after 5-7 days. The obtained crystals are suitable for single crystal x-ray diffraction measurement.

Physical measurements

Elemental analyses for C, H and N were performed with an Elementar Vario EL III analytic instrument. Powder X-ray diffraction (PXRD) data were collected on a Bruker D8 diffractometer with Cu Kα radiation (λ = 1.5418 Å). FT-IR spectra were recorded on an IF66V FT-IR (4000-400 cm^{-1}) spectrophotometer with KBr pellets. Differential scanning calorimetry (DSC) was carried out on Pyris 1 power-compensation differential scanning calorimeter in the range 98-310 K for **β**-crystals and the warming/cooling rate is 10 K·min^{-1} during the thermal cycles. Magnetic susceptibilities were measured on a Quantum Design MPMS-5 superconducting quantum interference device (SQUID) magnetometer over the temperature range 1.8-300 K. The measurements of temperature and frequency dependent dielectric constants and dielectric loss were carried out employing a concept 80 system (Novocontrol, Germany) in the temperature range 123-373 K (from -150 to 100°C), the sample prepared in the form of pellet with 6.0 mm diameter and 1.8 mm thickness was sandwiched between two parallel copper electrodes and the ac frequencies span from 1 Hz to 10^7 Hz.

X-ray crystallography. Two β-crystals were respectively selected to be centered on an Oxford Diffraction Xcalibur diffractometer equipped with a Sapphire 3 CCD detector and a graphite monochromated Mo Kα (λ = 0.71073 Å) owing to the crystal quality becomes bad in the cooling process. Measurements were performed at 293, 250, 220, 200, 165, 145, 125 (using one crystal) and 100 K (using another crystal) in the cooling process. The data collection routine, unit cell refinement, and data processing were carried out with the program CrysAlis.[15] Structures were solved by the direct method and refined by the full-matrix least-squares procedure on F^2 using SHELXL-97 program.[16] The non-Hydrogen atoms were anisotropically refined using the full-matrix least-square method on F^2 in the refinements of crystal structures at 293, 250, 220, 165, 145, 125 and 100 K. Disorder models were used for the CF_3 group in the structure refinements of β-crystal at 293, 250, 220 and 200 K. Each fluorine atom in the disordered CF_3 groups was assumed to have three possible sites and the occupied factors were refined for each site for the crystal structures at 293 and 250 K as well as have two possible sites and the occupied factors were refined for each site for the crystal structure at 220 K. All H atoms were placed at calculated positions (C-H = 0.93 Å for the pyridyl/phenyl rings and 0.97 Å for the methylene group) and refined riding on the parent atoms with $U(H) = 1.2U\mathrm{eq}$ for the structures besides that at 200 K. The crystallographic details about data collection and structural refinement at different temperatures (besides 200 K) are summarized in Table 1 and Table 2.

Results and discussion

Controlled growth of α- and β-crystals. The solvent nature affects strongly the procedures of both nucleation and growth of a crystalline phase, thus, the selectivity of crystalline phase can be realized using a suitable crystallization solvent. Both α- and β-crystals can be obtained using slow evaporation of the saturated solution of **1** at ambient temperature or slow cooling the saturated solution from room temperature (~25 °C) to 4 °C in a refrigerator. The α-crystals can be easily obtained using acetonitrile or acetone with A.R. grade as solvent. In contrast, the β-crystals only formed in the acetonitrile or acetone solution with a little amount of isopropanol. The exact mechanism what role the trace amount of isopropanol does play in the formation of β-crystals is not clear at the present stage. The phase purity of α-crystals and β-crystals was inspected by means of powder X-ray diffraction technique, the experimental diffraction patterns, displayed in Figure 1 (2θ = 5-22°) and Figure S1 (2θ = 5-50°), are in agreement well to the corresponding simulated ones for both α-crystals and β-crystals. It is worth mentioned that the phase transition occurred in α-crystal and β-crystal falls within the different temperature interval and is associated with a thermal anomaly in DSC plot, but the thermal anomaly in α-crystal was not observed in the DSC plot of β-crystal (ref. next section) and vice versa. These results indicate both α-crystals and β-crystals we obtained show high purity.

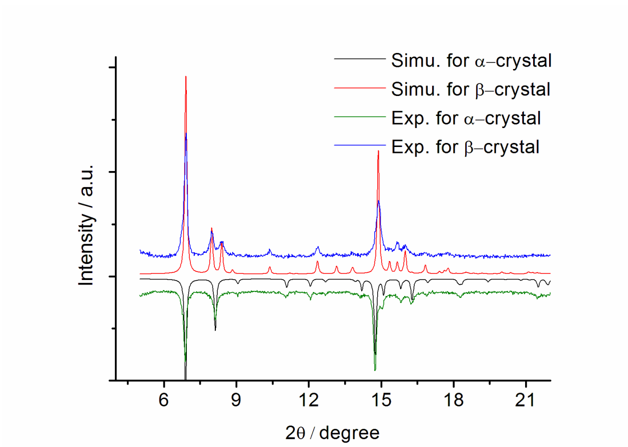

Figure 1 Experimental and simulated PXRD patterns of α-crystal and β-crystal at room temperature, where the characteristic diffraction at 2θ = 8.4° in the PRXD profile of β-crystal is not observed in the PXRD profile of α-crystal.

Differential scanning calorimetry (DSC). As our previously reported, the α-crystal undergoes a structural phase transition around 159 K, upon cooling, with a ~49 K hysteresis loop, while the β-crystal experiences two structural phase transitions in the narrow temperature interval of 190-217 K, which are confirmed by DSC measurements. As displayed in Figure 2, two visible endothermic events emerge in the heating regime in the 98-310 K range. One endothermic transition shows the peak temperature $T_{Peak} \approx 196$ K in the heating process, corresponding to an exothermic transition takes place at $T_{Peak} \approx 190$ K in the cooling run with $\Delta T \approx 6$ K. Another endothermic transition undergoes at $T_{Peak} \approx 217$ K in the heating regime, and the corresponding exothermic transition appears at $T_{Peak} \approx 206$ K with $\Delta T \approx 11$ K in the cooling regime. Two phase transitions are reversible and no sizable peak shift was observed for the endothermic and exothermic events in the successive thermal cycles. The enthalpies and entropies are estimated to be 198.2 $J{\cdot}mol^{-1}$ and 1.0 $J{\cdot}K^{-1}{\cdot}mol^{-1}$ between the low-temperature (LT) and intermediate (IT) phases *versus* 452.8 $J{\cdot}mol^{-1}$ and 2.1 $J{\cdot}K^{-1}{\cdot}mol^{-1}$ between the IT and high-temperature (HT) phases. These thermodynamic parameters are small for the crystalline phase transformation but fall within the range observed in most organic crystals.[17]

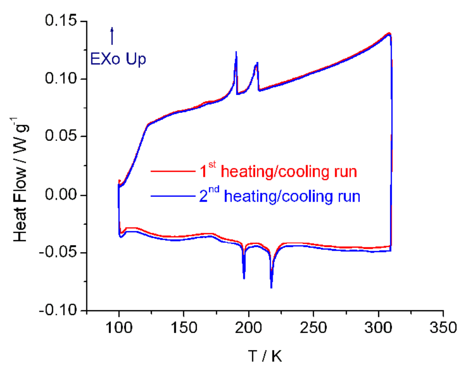

Figure 2 DSC curves for β-crystals. The red and blue solid lines represent the first and the second heating/cooling cycles, respectively.

The investigations of variable temperature single crystal structures disclosed that two phase transitions show the step-wise dynamic orientation motion of a part of anions and cations but the structural phase transitions are accompanied by change in neither the crystallographic space group nor the occupied Wyckoff positions, thus, two phase transitions β-crystal experienced, from the structural viewpoint, are categorized as "isostructural phase transitions" (IPTs).[18] The crystal structure of β-crystal was determined at 293, 250 and 220 K for the HT phase, at 200 K for the IT phase and at 165, 145, 125 and 100 K for the LT phase. We only give the detailed description for the crystal structures at 220 K for the HT phase, at 200 K for the IT phase and at 165 K for the LT phase below, and the crystal structures at other temperatures are summarized in ESI.

Crystal structure of β-crystal in HT phase at 220 K. The β-crystal belongs to triclinic space group P-1 in HT, IT and LT three crystalline phases. An asymmetric unit consists of two pairs of $[Ni(mnt)_2]^-$ anions and 4'-CF_3bzPy$^+$ cations in HT phase (Figure 3). However, an asymmetric unit contains one pair of $[Ni(mnt)_2]^-$ anion and 4'-CF_3bzPy$^+$ cation in α-crystal.[12] Two differently planar anions are almost parallel to each other with a dihedral angle of 2.5° where the mean-molecule plane of anion is defined through four coordination S atoms. The phenyl rings in the different cations are also approximately parallel to each other with a dihedral angle of 3.9° at 220 K. The bond lengths and bond angles in two planar anions, summarized in Table S1, are in good agreement with the values in α-crystal.[12] The bond lengths and bond angles in two crystallographically inequivalent cations fall within the expected values and are comparable to those in α-crystal.[12] The characteristic dihedral angles in two Λ-shaped 4'-CF_3BzPy$^+$ moieties are 69.6° (71.7°) between the phenyl and pyridyl rings, 87.7° (85.9°) between the reference plane N9/C22/C23 (N10/C32/C36) and the phenyl ring as well as 88.6° (82.7°) between the reference plane N9/C22/C23 (N10/C35/C36) and the pyridyl ring for the N9 (N10) cation. These dihedral angles are quite close to the corresponding values in α-crystal.[12] The CF_3 groups show structurally disordered and each fluorine atom was assumed to have two possible sites, the structural refinement gave the occupied factors 0.560/0.440 for F1F2F3/F1'F2'F3' and 0.479/0.521 for F4F5F6/F4'F5'F6'.

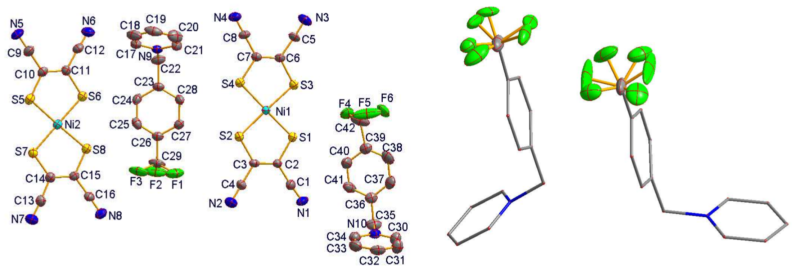

Figure 3 (a) ORTEP view with non-hydrogen atom labeling and thermal ellipsoids drawn at the 20% probability level (b) the structurally disordered CF_3 groups for the crystal in **β** phase at 220 K (The H atoms are omitted for clarity).

The anions and cations form the mixed stacks with alternating anion dimers and cation dimers in **α**-crystal,[12] while the segregated stacks in **β**-crystal (as displayed in Figure 4a). The anions are aligned in the manner of …Ni1/Ni1/Ni2/Ni2… (see Figure 4b) along the *c*-axis direction, with three types of adjacent Ni…Ni distances ($d_{Ni1…Ni1}$ = 3.999 Å, $d_{Ni1…Ni2}$ = 4.466 Å and $d_{Ni2…Ni2}$ = 3.997Å) and the distances of $d_{Ni1…Ni1}$ and $d_{Ni2…Ni2}$ are fairly close to each other within an anion stack. The cations are arranged in the fashion of …cation(N9)/cation(N9)/cation(N10)/ cation(N10)…along the *c*-axis direction, with three types of adjacent centroid-to-centroid distances between the face-to-face phenyl rings ($d_{N9…N9}$ = 4.610 Å, $d_{N9…N10}$ = 4.299 Å and $d_{N10…N10}$ = 4.864Å) within a cation stack (Figure 4c).

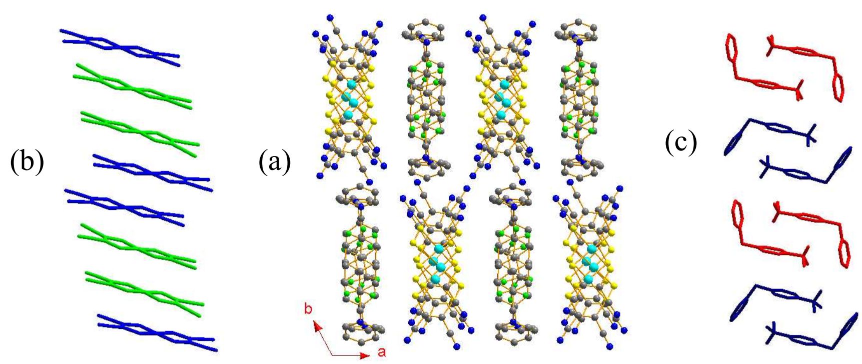

Figure 4 (a) Packing structure of **β**-crystal at 220 K viewed along the crystallographic *c*-axis (b) the anion stack where green and blue specimens represent the anions with Ni1 and Ni2 (c) cation stack where navy and red specimens represent the cations with

N9 and N10 (The H atoms are omitted for clarity).

Crystal structures in IT and LT phases. When the **β**-crystal is cooled from 220 to 200 K, a phase transformation occurs, which leads to the crystal changing from the room-temperature P-1 triclinic cell to another P-1 triclinic cell.[19] On passing through the phase transition, the *b*- and *c*-axes shorten, while the *a*-axis lengthens; the cell volumes together with the β and γ angles shrinks, whereas the α angle increase with respect to the cell at 220 K. It is noted that the Ni1 anion together with the N9 cation have lost the short-range ordering and split into two sites in IT phase, the structural refinement gave the occupied factors 0.503/0.497 for the disordered anion and 0.484/0.516 for the disordered cation and the occupied factor for each site is close to 0.5. Generally, a crystal shows the dynamic structural disorder in high temperature and becomes structural order upon cooling. To the best of our knowledge, the **β**-crystal is the first example which shows the structural order in high temperature but structural disorder in low temperature. As shown in Figure 5a, a transverse offset occurs between two orientationally disordered anions and a significant rotation emerges between two orientationally disordered cations, resulting in two phenyl rings in the cations containing N9' and N9 making a dihedral angle of 34.1°. It is very common that the components in a crystal lose short-range ordering across a structural transformation from low to high temperature phase, in contrast, the situation that the components in a crystal show orientationally disordered from high to low temperature is very rare and really interesting.

Upon cooling from 200 K to 165 K, the **β**-crystal undergoes the second isostructural phase transition. As displayed in Figure 5b, two crystallographically different anions and two cations show fully ordered in the LT phase and this situation is analogous to that of **α**-crystal in LT phase. The mean-molecule planes, defined respectively through their four coordination S atoms, between two different planar anions make a dihedral angle of 3.9°. The phenyl rings in two crystallographically different cations build a dihedral angle of 25.6° at 165 K. These dihedral angles are drastically different from those in HT phase. There are three different distances between the adjacent Ni…Ni in a …Ni1/Ni1/Ni2/Ni2… anion stack, with $d_{Ni1…Ni1}$ = 4.008 Å, $d_{Ni1…Ni2}$ = 4.495 Å and $d_{Ni2…Ni2}$ = 3.918Å. By comparison of the HT phase, the distances $d_{Ni1…Ni}$ and $d_{Ni1…Ni2}$ show a little bit expansion, while the distance $d_{Ni2…Ni2}$ exhibits slight reduction. There are three different centroid-to-centroid distances between the face-to-face phenyl rings within a …cation(N9)/cation(N9)/cation(N10)/cation(N10)…cation stack in HT phase, however, five different centroid-to-centroid distances $d_{N9…N9}$ = 4.625 Å, $d_{N10…N10}$ = 4.593Å and three different $d_{N9…N10}$ = 4.119, 4.489 and 4.582 Å in LT phase owing to the orientation change of one crystallographically different cation (see Table 3).

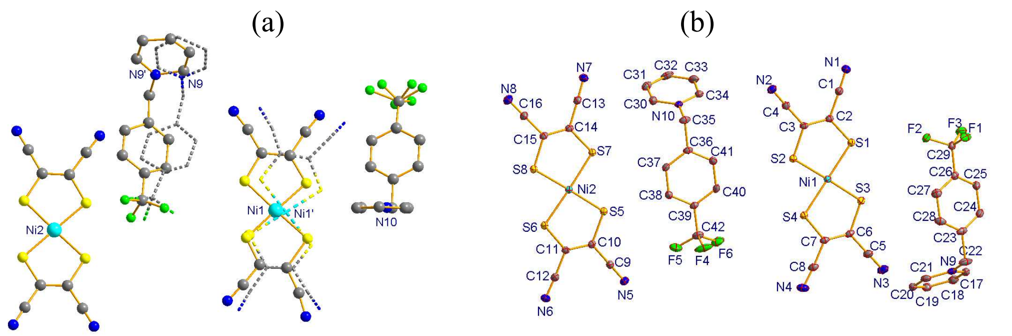

Figure 5 (a) Illustration for orientationally disordered anion and cation in IT phase at 200 K (b) ORTEP view with non-hydrogen atom labeling and thermal ellipsoids drawn at the 20% probability level in LT phase at 165 K (The H atoms are omitted for clarity).

Molecule orientation and stack variation across the structural phase transitions. As analyzed above, it can be found that the orientation motion of Ni1 anion and N9 cation play an important role in two isostructural phase transitions. The comparative views showing the dynamic orientation motion of both anion and cation are displayed in Figure 6a and Figure 6b, respectively. The Ni2 anion and N10 cation (excluding three F atoms) show fully ordered in the HT, IT and LT phases. With respect to the ordered Ni2 anion and N10 cation, the orientation change undergoes via the transverse slippage of about one half Ni1 anions as well as through the rotation of phenyl ring of about one half N9 cations from the HT to IT phase. The remaining one half Ni1 anions and N9 cations fulfilled the orientation change by means of the similar transverse slippage or rotation of phenyl ring from the IT to LT phase. The step-wise orientation variation of both Ni1 anion and N9 cation give rise to the change of anion and cation stacks, which are respectively shown in Figure 6c and Figure 6d, from the HT, passing through the IT, to the LT phase.

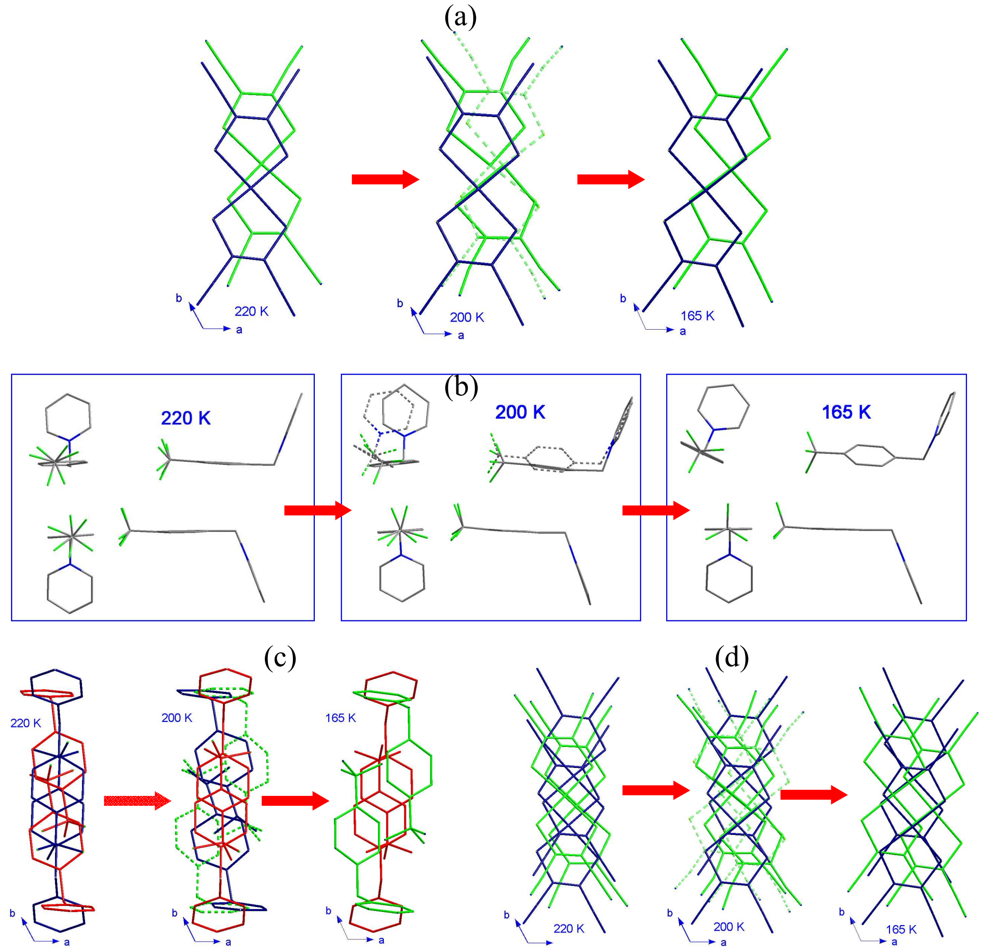

Figure 6 Illustration for (a, b) the relative orientation change of N9 cation and Ni1 anion with respect to the fully ordered N10 cation and Ni2 anion (c, d) the cation and anion stacks change across two isostructural phase transitions.

The orientation motions of anions and cations result in the cell parameters taking place the discontinue changes. As displayed in Figure 7, the length shrinks linearly with decreasing temperature for *a*-, *b*- and *c*-axes above 220 K; drops abruptly for *b*- and *c*-axes, while jumps for *a*-axis below 220 K. The lengths for all three crystallographic axes exhibit uniform contraction again when temperature is below 165 K. The no-smooth changes of cell parameters in 165-220 K, especially for three crystallographic axes, cell volume and α angle, are in agreement with the facts two phase transitions undergo in this temperature region.

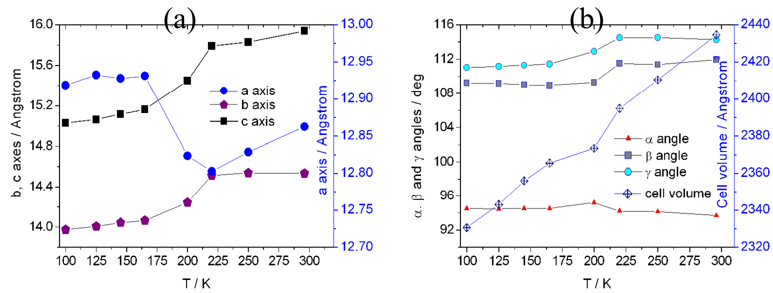

Figure 7 Temperature dependent cell parameters (a) *a*, *b* and *c*-axes (b) α, β, γ angles and cell volume V for **β**-crystal in 100–293 K temperature range.

Magnetic Property. The χ_m *vs*. *T* plots of **β**-crystal in the 1.8-300 K range are displayed in Figure 8a, where the χ_m represents the molar magnetic susceptibility with one $[Ni(mnt)_2]^-$ per formula unit. Two-step hysteretic magnetic phase transitions are observed with $T_{C1\downarrow} \approx 189.7$ K, $T_{C1\uparrow} \approx 194.5$ K and $\Delta T_1 \approx \sim 4.8$ K for the transition between IT and LT phases; with $T_{C2\downarrow} \approx 204.8$ K, $T_{C2\uparrow} \approx 214.1$ K and $\Delta T_2 \approx \sim 9.3$ K for the transition between HT and IT phases (ref. Figure 8b). The critical temperatures observed from magnetic measurements are comparable to those from DSC technique.

As mentioned in the crystal structure analyses, there are three clearly different Ni…Ni distances between the adjacent anions within a stack in the LT phase, the magnetic susceptibility data in the LT phase is difficult to be theoretically analyzed owing to lacking of the suitable function of magnetic susceptibility as the temperature for a spin chain system with three exchange constants, but we can estimated the amount of magnetic impurity using the Curie-Weiss law and the temperature independent magnetic susceptibility χ_0; the χ_0 term includes the diamagnetism contributed from the atoms core of molecules and the possible temperature-independent van Vleck-type paramagnetic susceptibility originated from the coupling of the ground and excited states through a magnetic field.[20]

$$\chi_m = \frac{C}{T-\theta} + \chi_0 \qquad (1)$$

The best fit, using Eq.(1), was undertaken for the magnetic susceptibility data in the 1.8-82 K range to give the parameters C = 2.9(5)×10^{-3} emu·K·mol^{-1}, θ = 0.01(4) K and χ_0 = -9.0(4)×10^{-5} emu·mol^{-1} and the square of the correlation coefficient R^2 = 0.998. A fraction of ~0.77% of S = ½ magnetic impurities is estimated from the fitted Curie constant.

The crystal structure analysis demonstrated that there are three types of Ni…Ni neighbors within a stack in the HT phase, namely, Ni1…Ni1, Ni1…Ni2 and Ni2…Ni2, but the distances of $d_{Ni1\ldots Ni1}$ and $d_{Ni2\ldots Ni2}$ are accidentally equal to each other, as a result, an anion stack can be considered as an alternating spin chain with two magnetic exchange constants in the HT phase. As an approximation, an S = ½ antiferromagnetic Heisenberg linear chain model was chosen for the fits of the temperature dependent magnetic susceptibility of **β**-crystals in the HT phase. The spin Hamiltonian for the Heisenberg alternating linear chain may be written as

$$\hat{H} = -2J\sum_{i=1}^{n/2}[\hat{S}_{2j-1}\hat{S}_{2j} + \alpha\hat{S}_{2j}\hat{S}_{2j+1}] \qquad (2)$$

Where J is the exchange constant between a spin and its left neighbor and αJ is the exchange constant between a spin and its right neighbor. For an antiferromagnetic exchange system (J < 0 and 0 ≤ α ≤ 1), extremely, when α = 0 the alternating linear chain model is simplified to the dimer model with pairwise interactions and when α = 1 the alternating linear chain model to the regular linear-chain model.[21-23] Based on the spin Hamiltonian in Eq.(2), the molar magnetic susceptibility as a function of temperature for an S = ½ Heisenberg antiferromagnetic linear chain, which is deduced from the cluster approach, can be expressed as

$$\chi_{chain} = \frac{Ng^2\mu_B^2}{k_B T}\cdot\frac{A + Bx + cx^2}{1 + Dx + Ex^2 + Fx^3} \qquad (3)$$

Where x = |J|/k_BT. The Eq.(3), with two sets of parameters A-F for the alternating-exchange linear spin chain, is valid for k_BT/|J| ≥ 0.5 and J ≤ 0,[22] while, with one set of parameters A-F for the regular linear spin chain, is suitable for

$k_BT_{max}/|J| = 1.282$ and $\chi_{max}|J|/Ng^2\mu_B^2 = 0.07346$.[23] The experimental molar magnetic susceptibility in the HT phase is given in Eq. (4) if the magnetic susceptibility contributions from the paramagnetic impurity (which originates from the lattice defects), molecular diamagnetism of atoms core and the possible van Vleck-type temperature-independent paramagnetism are further considered.

$$\chi_m = \chi_{chain} + \frac{C}{T-\theta} + \chi_0 \qquad (4)$$

The fit was performed for the magnetic susceptibility data over the temperature range 210-300 K using Eq. (4), and the C, θ and χ_0 parameters are set to be equal to the values obtained from magnetic susceptibility fit in the LT phase. The best fit yielded the parameters α = 0.04(1) and J/k_B = 219.3(6) K with g = 2.017[24] fixed and the square of the correlation coefficient R^2 = 0.944.

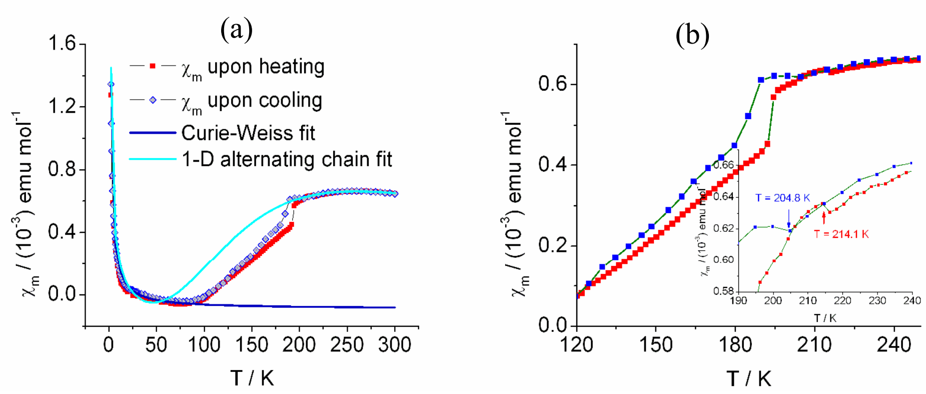

Figure 8 (a) χ_m vs T for **β**-crystals, where the light-blue and the red solid squares represent magnetic susceptibility data upon cooling and heating (b) the enlarged sections show the thermal hysteresis effects for two magnetic phase transitions.

Dielectric property. The temperature dependent dielectric permittivity ε' and loss $\tan\delta$ are shown in Figure 9a and 9b, respectively. Although two hysteretic magnetic phase transitions are coupled with the structural phase transitions, there is absent dielectric anomaly in the structural phase transition temperature region. With the increase in temperature (above 220 K), the dielectric dispersion is observed in the low-frequency regime and this is due to the mobility of polar CF_3 groups begin to increase (the CF_3 groups show structural disorder in both IT and HT phase) and further confirmed by the observation of the dielectric loss being larger as the temperature is increased.

The dielectric permittivity ε' and loss $\tan\delta$ as a function of frequency are displayed in Figure 9c at selected temperatures. At high temperatures, the dielectric permittivity drop rapidly with increasing frequency to 10^3 Hz, This result indicates that the dynamic dipole motion cannot follow the quickly switching of the applied electrical field at higher frequencies (f > 10^3 Hz). The dielectric permittivity is almost constant ($\varepsilon' \approx 24$) when the frequency of applied ac electrical field is more than 10^4 Hz. A dielectric loss peak becomes visible between the temperatures of 213 and 303 K. The maximum of dielectric loss peak in the plot of $\tan(\delta)$ versus f shifts toward higher frequencies with increasing temperature. This behavior is typical of a thermally assisted dielectric relaxation. Each of the four dielectric relaxation mechanisms has a typical relaxation frequency. Dielectric relaxation originated from electronic transitions or molecular vibrations has a frequency above 10^{12} Hz; while slow dielectric relaxations originated from dipole motion or ionic polarization occur in the range 10^2–10^{10} Hz. Thus, the dielectric relaxations in the frequency regime below 10^3 Hz observed in β-crystal arises probably from dipole motion of dynamically disordering CF_3 groups.

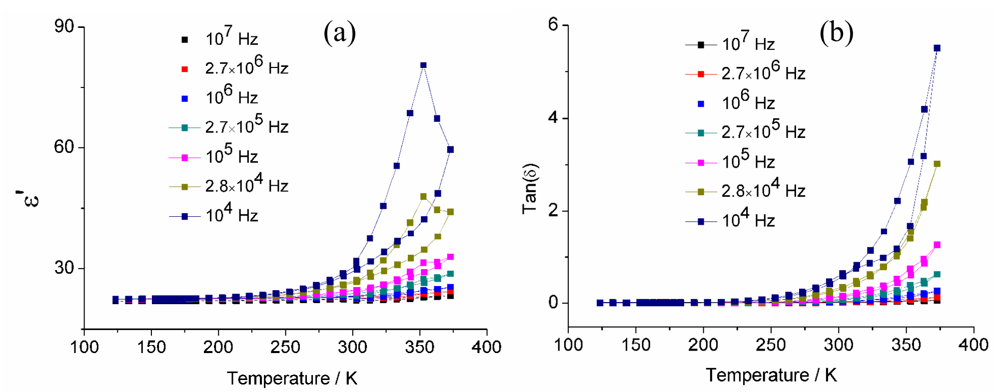

(c) (d)

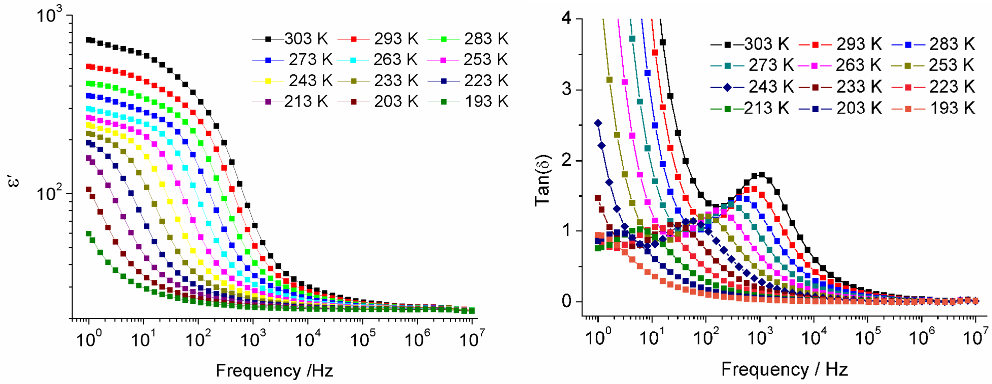

Figure 9 (a, b) Temperature and (c, d) frequency dependences of ε′ and tan(δ) in the 193-303 range K for **β**-crystal.

We further analyze the macroscopic relaxation time and potential barrier according to the following empirical Arrhenius relationship

$$\tau = \tau_0 \exp(\frac{E_a}{k_B T}) \qquad (5)$$

Where $\tau = 1/f_{max}$ and f_{max} is the frequency at maximum in the tan(δ) versus f plot at a selected temperature, τ_0 represents the characteristic macroscopic relaxation time, and E_a is so-called the activation energy or potential barrier. The best fits using Eq.(5) gave the following parameters (see Figure 10): E_a = 28.7 kJ·mol^{-1} with corresponding macroscopic relaxation time (τ_0) of 1.7×10^{-8} s.

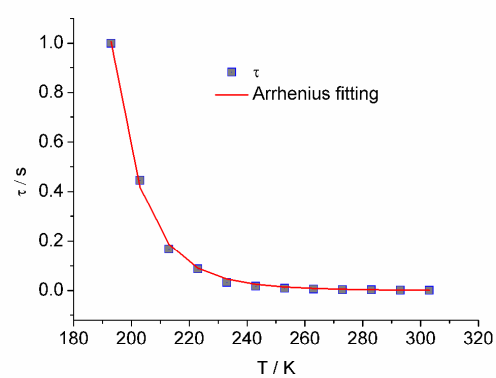

Figure 10 Plot of τ versus T for **β**-crystal in 193-303 range K.

Most dielectric materials behave differently than the Debye response. Thus, it is necessary to modify the empirical expression representing the Cole-Cole plot. One such a modification was proposed by Cole and Cole[25] and is given by:

$$\varepsilon^* = \varepsilon_\infty + \frac{\varepsilon_0 - \varepsilon_\infty}{1+(i\omega\tau)^{1-\alpha}} \qquad (6)$$

Where ε_0 is the static dielectric permittivity, ε_∞ is the dielectric permittivity at theoretically infinitely high frequencies, τ is the relaxation time, and α is related to the dispersion of the relaxation processes ($0 \leq \alpha \leq 1$). Figure 11 shows the Cole-Cole plots of the relaxation process for β-crystal at selected temperatures. The best fits were undertaken for the plots of imaginary part (ε'') versus real part (ε') of dielectric permittivity to yield the parameters ε_0, ε_∞, and α at the selected temperatures, which are summarized in Table 4. The relatively large α (= 0.19-0.25) values suggest that the dielectric relaxation processes show the moderate distribution of the relaxation time and depart from the Debye dielectric response model.

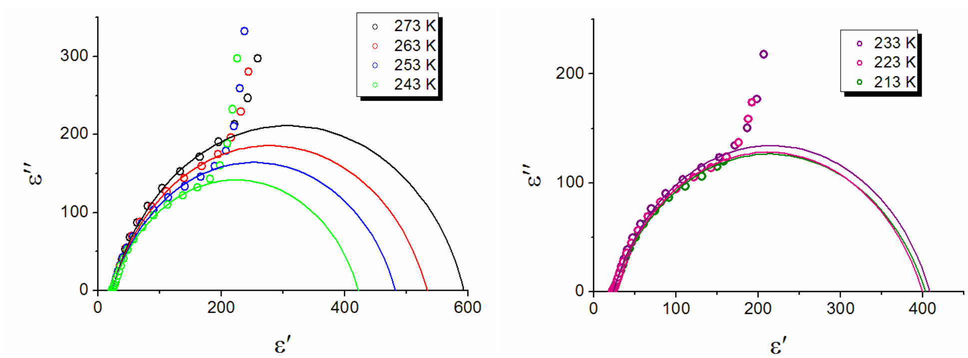

Figure 11 Selected Cole-Cole plots from 213 to 273 K for β-crystal.

Conclusion

In summary, we investigated the crystal structures at different temperatures, magnetic and dielectric properties for the second polymorph, β-crystal, of the nickel-dithiolene compound [4'-CF_3bzPy][$Ni(mnt)_2$]. Two reversible isostructural phase transitions undergo in the narrow temperature region (190-217 K) in the β-crystal, which are driven by the novel orientation motion of anion and cation, which result in two hysteretic magnetic phase transitions. There is absent dielectric anomaly in the structural transformation temperature interval, whereas a dielectric relaxation emerges in the HT phase and this is related to the dipole motion of disordered polar

CF_3 groups in the cations under an ac electrical field.

Acknowledgements

Authors thank the Priority Academic Program Development of Jiangsu Higher Education Institutions, the Science and Technology Department of Jiangsu Province and National Natural Science Foundation of China for financial support (grant Nos.: 21071080, 91122011 and 21271103).

Notes and References

1. a) D. Braga, F. Grepioni, L. Maini, M. Polito, *Struct. Bond.* **2009**, *132*, 25-50; b) J. Bernstein, Polymorphism in Molecular Crystals, Clarendon Press: Oxford, 2002; c) J. D. Dunitz, J. Bernstein, *Acc. Chem. Res.* **1995**, *28*, 193-200.
2. a) B. Rodríguez-Spong, C. P. Price, A. Jayasankar, A. J. Matzger, N. Rodríguez-Hornedo, *Adv. Drug Delivery Rev.* **2004**, *56*, 241-274; b) R. J. Davey, *Chem. Commun.* **2003**, 1463-1467.
3. a) C. Avendano, Z. Y. Zhang, A. Ota, H. H. Zhao, K. R. Dunbar, *Angew. Chem.Int. Ed.* **2011**, *50*, 6543-6547; b) N. K. Nath, H. Aggarwal, A. Nangia, *Cryst.Growth & Des.* **2011**, *11*, 967-971; c) T. S. Thakur, R. Sathishkumar, A. G. Dikundwar, T. N. Guru Row, G. R. Desiraju, *Cryst. Growth & Des*. **2010**, *10*, 4246-4249; d) M. Fettouhi, L. Ouahab, M. Hagiwara, E. Codjovi, O. Kahn, H. Constant-Machado, F. Varret, *Inorg. Chem.* **1995**, *34*, 4152-4159 ; e) E. Laukhina, J. Vidal-Gancedo, V. Laukhin, J. Veciana, I. Chuev, V. Tkacheva, K. Wurst, C. Rovira, *J. Am. Chem. Soc.* **2003**, *125*, 3948-3953.
4. a) B. Zhang, Y. Zhang, D. B. Zhu, *Chem. Commun.* **2012**, 197-199; b) B. Zhang, Z. M.Wang, Y. Zhang, H. Kobayashi, M. Kurmoo, T. Mori, F. L. Pratt, K. Inoue, D. B. Zhu, *Polyhedron* **2007**, *26*, 1800-1804; c) H. L. Peng, C. B. Ran, Z. F. Liu, Y. Z. Long, Z. M. Wang, Z. Q. Yu, H. L. Sun, Y. G. Wei, S. Gao, Z. J. Chen, E. Q. Chen, *J. Phys. Chem. C* **2008**, *112*, 11001-11006; d) B. Zhou, H. Yajima, A. Kobayashi, Y. Okano, H. Tanaka, T. Kumashiro, E. Nishibori, H. Sawa, H. Kobayashi, *Inorg. Chem.* **2010**, *49*, 6740-6747.
5. a) A. T. Coomber, D. Beljonne, R. H. Friend, J. L. Brédas, A. Charlton, N. Robertson, A. E. Underhill, M. Kurmoo, P. Day, *Nature* **1996**, *380*, 144-146; b) O. Jeannin, R. Clérac, M. Fourmigué, *J. Am. Chem. Soc.* **2006**, *128*, 14649-14656; c) M. Fourmigué, *Acc. Chem. Res.* **2004**, *37*, 179-186; d) R. D. Willett, C. J. Gómez-Garcí, B. L. Ramakrishna, B. Twamley, *Polyhedron* **2005**, *24*, 2232-223; e) R. A. L. Silva, A. I. S. Neves, E. B. Lopes, I. C. Santos, J. T. Coutinho, L. C. J. Pereira, C. Rovira, M. Almeida, D. Belo, *Inorg. Chem.* **2013**, 52, 5300-5306.

6. a) T. Akutagawa, T. Hasegawa, T. Nakamura, T. Inabe, G. Saito, *Chem. Eur. J.* **2002**, *8*, 4402-4411; b) T. Akutagawa, S. Takeda, T. Hasegawa, T. Nakamura, *J. Am. Chem. Soc.* **2004**, *126*, 291-294; c) H. Kobayashi, A. Kobayashi, H. Tajima, *Chem. Asian J.* **2011**, *6*, 1688-1704; d) B. Zhou, A. Kobayashi, Y. Okano, T. Nakashima, S. Aoyagi, E. Nishibori, M. Sakata, M. Tokumoto, H. Kobayashi, *Adv. Mater.* **2009**, *21*, 3596-3600.

7. a) J. A. Schlueter, L. Wiehl, H. Park, M. de Souza, M. Lang, H. J. Koo, M. H. Whangbo, *J. Am. Chem. Soc.* **2010**, *132*, 16308-16310; b) C. Rovira, *Chem. Rev.* **2004**, *104*, 5289-5318; b) F. Wudl, D. Wobschall, E. J. Hufnagel, *J. Am. Chem. Soc.* **1972**, *94*, 670-672; c) J. Ferraris, D. O. Cowan, V. Walatka, J. H. Perlstein, *J. Am. Chem. Soc.* **1973**, *95*, 948-949; J. Lieffrig, O. Jeannin, T. Guizouarn, P. Auban-Senzier, M. Fourmigué, *Cryst. Grow. & Des.* **2012**, *12*, 4248-4257; d)T. Shirahata, K. Shiratori, S. Kumeta, T. Kawamoto, T. Ishikawa, S. Y. Koshihara, Y. Nakano, H. Yamochi, Y. Misaki, T. Mori, *J. Am. Chem. Soc.* **2012**, *134*, 13330-13340.

8. a) B. Zhang, Z. Wang, H. Fujiwara, H. Kobayashi, M. Kurmoo, K. Inoue, T. Mori, S. Gao, Y. Zhang, D. Zhu, *Adv. Mater.* 2005, **17**, 1988-1991; b) B. Zhang, M. Kurmoo, T. Mori, Y. Zhang, F. L. Pratt, D. Zhu, *Cryst. Grow. & Des.* 2010, **10**, 782-789.

9. a) S. Benjamin, S. Pagola, Z. Huba, E. Carpenter, T. Abdel-Fattah, *Synth. Met.* **2011**, *161*, 996-1000; b) R. Pfattner, M. Mas-Torrent, I. Bilotti, A. Brillante, S. Milita, F. Liscio, F. Biscarini, T. Marszalek, J. Ulanski, A. Nosal, M. Gazicki-Lipman, M. Leufgen, G. Schmidt, L. W. Molenkamp, V. Laukhin, J. E Veciana, C. Rovira, *Adv. Mater.* **2010**, *22*, 4198-4203; c) J. A. Schlueter, U. Geiser1, H. H. Wang1, J. L. Manson, *Phys. Status Solidi B* **2012**, *249*, 933-936.

10. Q. Ye, T. Akutagawa, N. Hoshino, T. Kikuchi, S. I. Noro, R. G. Xiong, T. Nakamura, *Cryst. Growth & Des.* **2011**, *11*, 4175-4182.

11. a) X. M. Ren, S. Nishihara, T. Akutagawa, S. Noro, T. Nakamura, *Inorg. Chem.* **2006**, *45*, 2229-2234; b) S. Q. Zang, X. M. Ren, Y. Su, Y. Song, W. J. Tong, Z. P. Ni, H. H. Zhao, S. Gao, Q. J. Meng, *Inorg. Chem.* **2009**, *48*, 9623-9630; c) W. B.

Pei, J. S. Wu, W. H. Ning, X. M. Ren, Z. F. Tian, Y. X. Sui, *Cryst. Grow. & Des.* **2012**, *12*, 2419-2426.

12. H. B. Duan, X. R. Chen, H. Yang, X. M. Ren, F. Xuan, S. M. Zhou, *Inorg. Chem.* **2013**, *52*, 3870-3877.
13. A. Davison, H. R. Holm, *Inorg. Synth.* **1967**, *10*, 8-33.
14. X. M. Ren, Q. J. Meng, Y. Song, C. S. Lu, C. J. Hu, *Inorg. Chem.* **2002**, 41, 5686-5692.
15. CrysAlis V1.171; Oxford Diffraction Ltd.: Wrocław, Poland, **2004**.
16. G. M. Sheldrick, SHELXL-97, Program for the Refinement of Crystal Structures; University of Gottingen: Gottingen, Germany, **1997**.
17. A. Gavezzotti, G. Filippini, *J. Am. Chem. Soc.* **1995**, *117*, 12299-12305.
18. R. A. Cowley, *Phys. Rev. B*, 1976, **13**, 4877-4885.
19. Notes: β-crystal data at 200 K. $C_{21}H_{11}F_3N_5NiS_4$, M_r= 577.30, triclinic, space group *P-1*, a = 12.8236(9) Å, b = 14.2423(9) Å, c = 15.4496(12) Å, α = 95.212(6)°, β = 109.302(7)°, γ = 112.911(6)°, V = 2373.5(3) Å^3, Z = 4 , ρ_{calcd}= 2.297 g cm^{-3}, μ = 5.243 mm^{-1}, 15619 reflections collected, 8832 independent reflections. The final R values were R_1 = 0.0782, wR_2 = 0.1971 for I > 2σ(I). R_1 = 0.1591, wR_2 = 0.2427 for all data. It is mentioned that the single crystal X-ray diffraction data at 200 K show a high R_{sigma} value in the cooling process; this is due to the heavily structural disordered. The structural refinement was performed to assume one pair anion-cation having two possible sites, respectively. The non-Hydrogen atoms were anisotropically refined using the full-matrix least-square method on F^2 besides all fluorine atoms. All H atoms were not added in the refinement.
20. J. H. Van Vleck, The Theory of Electric and Magnetic Susceptibilities, Oxford, London, **1932**.
21. J. Bonner, M. E. Fisher, *Phys. Rev. A* **1964**, *235*, 640-658.
22. J. W. Hall, W. E. Marsh, R. R. Weller, W. E. Hatfield, *Inorg. Chem.* **1981**, *20*, 1033-1037.
23. D. A. Tucker, P. S. White, K. L. Trojan, M. L. Kirk, W. E. Hatfield, *Inorg. Chem.*

1991, *30*, 823-826.

24. X. M. Ren, R. K. Kremer, Q. J. Meng, *J. Magn. Magn. Mater.* **2004**, *272-276*, 924-926.
25. K. S. Cole, R. H. Cole, *J. Chem. Phys.* **1941**, *9*, 341-351.

Table 1: Crystal data and structural refinements of β-crystal in HT phase at 293, 250 and 220 K

Temperature	293 K	250 K	220 K
Chemical formula		$C_{21}H_{11}F_3N_5NiS_4$	
Formula weight		577.30	
Wavelength (Å)		0.71073	
CCDC number	963774	963773	963772
Crystal system	triclinic	triclinic	triclinic
Space group	*P-1*	*P-1*	*P-1*
a (Å)	12.8612(7)	12.815(6)	12.8027(9)
b (Å)	14.5184(8)	14.539(7)	14.5132(10)
c (Å)	15.9549(9)	15.829(7)	15.7920(11)
α (°)	93.617(5)	94.155(6)	94.218(5)
β (°)	111.974(5)	111.363(5)	111.499(6)
γ (°)	114.279(5)	114.510(5)	114.488(7)
V(Å3) / Z	2434.0(3)/4	2410.5(19)/4	2394.8(3)/4
Density ($g\cdot cm^{-3}$)	1.576	1.591	1.601
Abs coeff. (mm^{-1})	1.183	1.195	1.202
F(000)	1164	1164	1164
Data collect θ range	3.00 -25.50	2.41-26.73	2.58-26.73
Index range	$-15\leq h \leq 15$	$-16\leq h \leq 16$	$-16\leq h \leq 16$
	$-17 \leq k \leq 16$	$-17 \leq k \leq 18$	$-18 \leq k \leq 18$
	$-19 \leq l \leq 19$	$-20 \leq l \leq 20$	$-19 \leq l \leq 19$
Reflns collected	24537	19748	17130
Independent reflns	9046	10034	9996
Data/restraints/parameters	9042/342/727	10034/138/669	9996/138/669
Goodness-of-fit on F^2	1.071	1.013	1.021
Final R indices [$I > 2\sigma(I)$]	$R_1 = 0.0781$	$R_1 = 0.0486$	$R_1 = 0.0634$
	$wR_2 = 0.2241$	$wR_2 = 0.1247$	$wR_2 = 0.1132$
R indices [All data]	$R_1 = 0.1093$	$R_1 = 0.0763$	$R_1 = 0.1400$
	$wR_2 = 0.2373$	$wR_2 = 0.1438$	$wR_2 = 0.1496$

$R_1 = \Sigma(||F_o|-|F_c||)/\Sigma|F_o|$, $wR_2 = \Sigma w(|F_o|^2-|F_c|^2)^2/\Sigma w\ (|F_o|^2)^2]^{1/2}$

Table 2: Crystal data and structural refinements of β-crystal in LT phases at 165, 145, 125 and 100 K

Temperature	165 K	145 K	125 K	100 K
Chemical formula	$C_{21}H_{11}F_3N_5NiS_4$			
Formula weight	577.30			
Wavelength (Å)	0.71073			
CCDC number	963771	963770	963769	963768
Crystal system	triclinic	triclinic	triclinic	triclinic
Space group	*P-1*	*P-1*	*P-1*	*P-1*
a (Å)	12.9314(4)	12.9281(4)	12.9505(10)	12.9083(13)
b (Å)	14.0640(4)	14.0427(5)	14.0017(7)	13.9442(14)
c (Å)	15.1632(5)	15.1169(6)	15.0589(12)	15.0273(15)
α (°)	94.518(3)	94.533(3)	94.534(6)	94.571(3)
β (°)	108.962(3)	109.027(3)	109.066(7)	109.244(3)
γ (°)	111.444(3)	111.286(3)	111.091(6)	110.955(3)
V($Å^3$) / Z	2365.57(12)/4	2355.98(15)/4	2347.3(3)/4	2324.2(4)/4
Density ($g·cm^{-3}$)	1.621	1.628	1.634	1.650
Abs coeff. (mm^{-1})	1.217	1.222	1.227	1.239
F(000)	1164	1164	1164	1164
Data collect θ range	2.92-27.00	2.93-27.00	2.88-27.00	1.47-27.51
Index range	$-16 \le h \le 14$ $-17 \le k \le 17$ $-17 \le l \le 19$	$-16 \le h \le 16$ $-17 \le k \le 17$ $-19 \le l \le 19$	$-16 \le h \le 16$ $-17 \le k \le 17$ $-18 \le l \le 19$	$-16 \le h \le 16$ $-18 \le k \le 18$ $-19 \le l \le 19$
Reflns collected	21671	23540	22248	33398
Independent reflns	10166	10141	10072	10521
Data/restraints/parameters	10166/0/613	10141/0/613	10072/0/613	10521 /0/613
Goodness-of-fit on F^2	1.010	1.017	0.964	1.001
Final R indices [I > 2σ(I)]	$R_1 = 0.0418$ $wR_2 = 0.0891$	$R_1 = 0.0399$ $wR_2 = 0.0864$	$R_1 = 0.0602$ $wR_2 = 0.1448$	$R_1 = 0.0369$ $wR_2 = 0.0763$
R indices [All data]	$R_1 = 0.0686$ $wR_2 = 0.0989$	$R_1 = 0.0620$ $wR_2 = 0.0944$	$R_1 = 0.0915$ $wR_2 = 0.1644$	$R_1 = 0.0660$ $wR_2 = 0.0859$

$R_1 = \Sigma(||F_o|-|F_c||)/\Sigma|F_o|$, $wR_2 = \Sigma w(|F_o|^2-|F_c|^2)^2/\Sigma w\,(|F_o|^2)^2]^{1/2}$

Table 3: The comparison of the important structural parameters of β-crystal between the HT, IT, LT phases

Structural Parameters	HT phase (220K)	IT phase (200K)	LT phase (165K)
$\mathbf{d_{Ni1\text{-}Ni1}}$ /Å	3.999	4.027	4.008
$\mathbf{d_{Ni1\text{-}Ni2}}$ /Å	4.466	4.560	4.495
$\mathbf{d_{Ni2\text{-}Ni2}}$ /Å	3.997	3.941	3.918
$\mathbf{d_{N9\text{-}N9}}$ /Å	4.610	4.967	4.625
$d_{N9\text{-}N10}$ /Å	4.299	4.129	4.119, 4.489, 4.582
$\mathbf{d_{N10\text{-}N10}}$ /Å	4.864	4.565	4.593
θ /° (dihedral angle)	3.9	3.9/32.4	25.6

Table 4: ε_0, ε_∞ and α parameters obtained from the best fits for β-crystal at the selected temperatures

Temp. / K	ε_0	ε_∞	α	R^2
273	593.27	23.04	0.19	0.99815
263	533.12	22.95	0.20	0.99813
253	481.97	22.88	0.21	0.99805
243	422.06	22.82	0.22	0.9978
233	408.71	22.77	0.23	0.99998
223	399.61	22.72	0.24	0.99801
213	403.58	22.69	0.25	0.99656

TOC

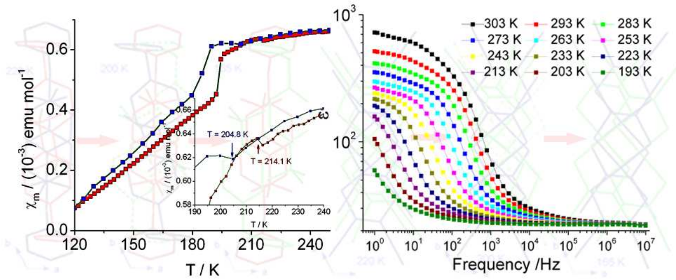

Step-wise orientation motions of ions result in two successively structural transitions, one of them is associated with hysteretic magnetic transition in a one-dimensional nickel-bis-dithiolene salt and dielectric relaxation occurs in high temperature region.